# Pathology Design for Surgical Training Simulators

Raimundo Sierra[1], Michael Bajka[2], and Gábor Székely[1]

[1] Computer Vision Group, ETH Zürich, Switzerland,
{rsierra, szekely}@vision.ee.ethz.ch
[2] Clinic of Gynecology, Dept. OB/GYN, University Hospital of Zürich, Switzerland

**Abstract.** Realistic generation of variable anatomical organ models and pathologies are crucial for a sophisticated surgical training simulator. A training scene needs to be different in every session in order to exhaust the full potential of virtual reality based training. We previously reported on a cellular automaton able to generate leiomyomas found in the uterine cavity. This paper presents an alternative approach for the design of macroscopic findings of pathologies and describes the incorporation of these models into a healthy virtual organ. The pathologies implemented are leiomyomas and polyps protruding to different extents into the uterine cavity. The results presented are part of a virtual reality based hysteroscopy simulator that is under development.

## 1 Introduction

In the last few years many surgical training simulators have been developed [6, 8, 9]. There is consensus that one of the main advantages of a training simulator is the ability to offer training on many different surgical scenes in a compressed period of time, thus increasing the experience of the trainee. Nevertheless, the generation of variable anatomical models of the healthy organ and the incorporation of pathologies have not been treated as a specific issue. Instead, today's simulators use single static organ models, usually derived from an exemplary anatomy such as an MRI dataset of a volunteer, a specially acquired high resolution dataset, or artificially created with CAD.

Our current research aims at the development of a hysteroscopy simulator. Hysteroscopy is the visualization of the inner surface of the uterus by performing a distension of the cavum uteri, realized through a single hull for manipulation and visualization. It makes minimal invasive surgery on the uterus possible and allows the physician to perform a specific treatment under organ saving conditions. Hysteroscopy is the second most often performed endoscopic procedure after laparoscopy in gynecology. Because of lack of alternatives, training is usually performed during actual interventions, with an experienced gynecologist.

A single organ model is inherently unable to represent an everyday situation of the operating site, thus obstructing the training effect of the simulator. The organs of any two patients will never be alike. Statistical anatomical models, for example those used for the incorporation of prior anatomical knowledge into the

segmentation process [3, 7] offer an appealing way to handle the variability of healthy human anatomy within the organ models used for simulation.

The other requirement for a reasonably realistic surgical simulator is the ability to offer training on a wide variety of pathological cases. The large number of possible pathologies as well as the enormous range of their manifestations makes a similar statistical approach unreasonable if not impossible. We are therefore exploring different approaches to model the pathologies.

We previously reported on a cellular automaton that is able to model different types of leiomyomas. A minimal set of rules was presented that simulates the growth process of a myoma. Thus, by successive and probabilistic application of the rules new myomas are generated [15]. The limitations of the cellular automaton become obvious when investigating pathologies like polyps. The interaction between the surface of the pathology and the healthy organ is an integral part of the growing process. Modeling of collisions in a cellular automaton is far more complex than in any surface based system.

In this work, a different strategy for the generation of pathologies found in the uterine cavity is described and their incorporation into the model of the healthy organ is presented. Instead of growing a pathology model every time a different manifestation is needed, the desired findings are directly designed. In a second step, the pathology is embedded in the healthy organ. Hysteroscopy being the target application, the most frequent pathologies visible from within the uterine cavity have been implemented, namely submucosal leiomyomas and polyps. The implementation of the first one allows for a direct comparison with the previously published approach. In addition, polyps are excellent candidates to discover the suitability and limitations of the different approaches, as they have significantly different properties than myomas.

## 2 Pathologies in the Uterine Cavity

Leiomyomas and polyps are both the cause of abnormal bleeding and the reason for the majority of hysteroscopic interventions. While the symptoms and the appearance of these pathologies might to some extent be similar, their treatment during hysteroscopy is completely different. Resecting a pedunculated myoma the same way as a polyp is removed can lead to serious problems during intervention.

### 2.1 Myoma Formation

Uterine leiomyomas are well-circumscribed, non-cancerous tumors arising from the myometrium of the uterus. They are found in 25-40% of women in their childbearing years and are classified by their location in the uterus. In hysteroscopy submucosal leiomyomas, both sessile and pedunculated, protruding to different extents into the cavity, are visible and treatable. As a myoma is composed of very dense fibrotic tissue, it has a much stronger tendency to keep its shape than any of the surrounding tissues. Therefore the myoma will be able to grow almost

independently from its surroundings and keep a spherical shape. The size of a myoma can range from a few millimeters up to several decimeters.

Removing a myoma is usually done by electric resection in small parts. A monopolar loop electrode is used to carve small strips that can subsequently be grasped and extracted from the cavity through the cervix. In doing so, it is crucial to keep the peduncle. Cutting off the peduncle of a myoma can lead to serious problems in hysteroscopy: the rigid sphere that forms the myoma will be floating like a ball in the cavity, making any further resection impossible.

### 2.2 Polyp Formation

Endometrial polyps are - like myomas - benign tumors. They are encountered most commonly in women between 40 and 50 years of age and occur relatively frequently after the menopause. The prevalence of polyps in the general population is about 24% [10].

As most polyps are small, they do not cause symptoms. The most common clinical presentation is abnormal bleeding, less frequently they are the cause of infertility. Two types of polyps are distinguished, one type originating from the corpus, the other from the cervix [14]. There is no classification based on the size or shape of a polyp.

Polyps originate as focal hyperplasias of the basalis and develop into benign, localized overgrowth of endometrial tissue covered by epithelium and containing a variable amount of glands, stroma, and blood vessels. These components make them - in contrast to myomas - very soft. Polyps may be broad-based and sessile, pedunculated, or attached to the endometrium by a slender stalk. Furthermore, they vary in size from 1.0 mm to a mass that fills and expands the entire uterine cavity. They rarely exceed 1.5 cm in diameter. Large polyps may extend down the endocervical canal or may even protrude into the vagina, being visible on physical examination. The surface is tan and glistening, but occasionally the tip or the entire polyp may be hemorrhagic or characterized by sufusions and petechiae due to irritation of infraction. Polyps are generally solitary, but about 20% are multiple. They may originate anywhere in the uterine cavity, but most occur in the fundus, usually in the cornual region.

The occurrence of carcinoma in benign polyps has been reported to be no more than 0.5%; however, polyps have been found in 12-34% of uteri with endometrial carcinoma. Polyps found in postmenopausal women are therefore always subject to histological investigation, as they are often a side effect of a carcinoma [1]. It is important to remove any polyp completely from the basis, otherwise there will always be a chance of relapse.

Hysteroscopy offers the accepted advantages of direct visualization, targeted biopsy and simultaneous complete surgical resection of polyps and myomas. Ultrasound often fails to accurately differentiate between polyps, hyperplasia and endometrial carcinoma. Hysteroscopy is more specific as a diagnostic tool in cases of post-menopausal bleeding and the combined use of hysteroscopy and biopsy leads to nearly 100% accuracy [16].

The hysteroscopic resection of a polyp - as opposed to the resection of a myoma - is best performed by picking the stem of the polyp and extruding it. Once the polyp is separated from the uterus, it can easily be pulled out of the cavity, as the soft tissue of the polyp can be squeezed through the cervix.

Table 1 summarizes the basic differences between myomas and polyps in the context of surgical training simulation. If polyps and myomas cannot be visually distinguished, haptic feedback can indicate the pathology.

**Table 1.** Fundamental differences between myomas and polyps

| Property | Myoma | Polyp |
|---|---|---|
| Origin | Myometrium | Endometrium |
| Tissue | Stiff | Soft |
| Shape | Spherical | Elongated |
| Resection | Carving | Extruding |

## 3 Skeleton Based Pathology Design

Almost a century ago, D'Arcy Thompson already identified the decisive role of axial growth processes in forming the shape of living objects [4]. The concept of local symmetries has later been shown to capture axial growth efficiently and can be handled by a coherent mathematical theory [2]. Local symmetries are described by skeletons, which are therefore a good tool for designing anatomical objects such as the pathologies under scrutiny. For axial growth, a skeleton can be approximated by of a set of connected axes that describe the geometry of the object, and a width $r$ associated with every position $p$ of every axis of the skeleton [13].

The design process is initiated by generating a skeleton $S$. Even though relatively complex growth patterns can theoretically emerge, only one main axis of growth can be identified in the presented pathologies. However, more complex geometrical structures are sometimes observed in polyps, e.g. in cases where the tip of the polyp seems to split. Yet, extreme tree-like branching does not occur. These small geometrical changes can be handled differently by specific application of the surface distortion, as shown below.

In an unconstrained environment, the growth process can be idealized to follow one straight axis. The restrictions imposed by the organ's shape are considered later in the post-processing steps of the design. The beginning of the skeleton is aligned with the origin of the coordinate system and the tip placed somewhere on the $z$-axis. The $z$-value represents the size of the pathology specified by the physician and scaled to the relative size of the organ. Using this orientation, the socket of the pathology lies on an virtual plane $\Sigma$ which coincides with the $xy$-plane.

The width function $r(p)$ is determined by a characteristic profile of the desired pathology. This profile is generated by a two dimensional non-uniform rational B-spline (NURBS) curve $C$ parameterized by $t \in [0..1]$ [5]. The control points of the curve $C$ have been empirically selected to produce profiles that match the descriptions and images of real pathologies. As one basic requirement for the generation of models for surgical simulators is the specification in medical terminology [15], the physician will select the desired pathology (myoma or polyp) as well as the size and width of the body and the peduncle. Consistency tests have to ensure meaningful values before transforming the specifications into the control points.

The profile is discretized at regular intervals of the parameter $t$. In the case of the polyp, two different radii can be specified to generate elliptical axial shapes. The profile is then scaled by $r_1 \cos(\varphi) + r_2 \sin(\varphi)$. This extension is not needed in the case of myomas, due to their spherical shapes. The surface $\Omega$ of the pathology is a 4-connected grid where its vertices are defined by the discrete angles $\varphi_i$ and the discrete positions $t_i$ of the profile. The resulting structure is open at the socket on the plane $\Sigma$.

In addition to the grid connections, every point $p \in \Omega$ is connected to its closest skeleton point, resulting in a segmentation of the skeleton at $z$-values corresponding to the projections of the $t_i$ positions of the profile. Additionally, a triangulation of the surface is defined for rendering purposes. All connections are modeled by springs. Three different stiffness factors are assigned to the following spring elements in increasing order: surface to surface, surface to skeleton and skeleton to skeleton.

Randomness is introduced by modulating the generated surface $\Omega$. The points $p$ on the surface are displaced in normal directions $\boldsymbol{n}_p$. The amount $d(p)$ of displacement is chosen such as to achieve a predefined global amplitude $a_0$ and frequency. The values $d(p)$ can be stored in a matrix $D$ since the surface $\Omega$ is a 4-connected grid. In principle, the values of every element $D_{ij}$ in the matrix can be randomly selected and the resulting matrix smoothed with a circular Gauss filter. The amplitude $a_0$ of the perturbation is additionally modulated with the radius $r(p)$ to avoid too large distortions at the peduncle:

$$d(p) = a_0 r(p) x$$

where $x$ is a uniformly distributed random variable in the range $[-1..1]$. The repeated application of this process with different amplitudes and filter-lengths leads to different perturbation patterns at different scales, allowing a simple interactive modification of the shape. In the actual implementation, the modulating and smoothing steps are unified for efficiency. Figure 1 illustrates the results of the process described for a polyp and a myoma.

## 4 Fusion of Pathology with Healthy Anatomy

Alternative tumor growth models place an initial seed for the pathology directly in the organ's model. Finite element analysis has been used to model the deformation of the organ induced by the growth process [11]. The application of

such concepts is coupled with the modeling of the growth processes inside the organ and thus not applicable in the current approaches. In both the cellular automaton and the skeleton method, the pathology models $M_{pathology}$ have to be combined with the organ model $M_{organ}$ after they have been generated.

A model $M$ is an entity associated with a certain representation. In the current context, $M_{organ}$ is an uterus represented by a triangulated, inner and outer surface oriented according to a patient specific coordinate system. In the case of the cellular automaton, $M_{CA}$ is a voxel based representation of different concentrations on which the rules are applied. The skeleton model $M_S$ of a pathology incorporates a surface representation with a local coordinate system at the origin of the pathology. The set $\mathcal{L}$ denotes a representation type, by convention labeled with the original model instance. Therefore $\mathcal{L}_{organ}$ is the set of models parameterized by a surface triangulation, whereas $\mathcal{L}_{pathology}$ is the set of models represented by voxels in the case of the cellular automaton and by surface triangulation in the case of the skeleton-based approach.

The combination of the organ and the pathology corresponds to a transformation $T : \mathcal{L}_a \rightarrow \mathcal{L}_b$ and additional operations on the models $M$. For the case of the cellular automaton this leads to

$$\mathcal{L}_{organ} \quad \xrightarrow{T_1} \quad \mathcal{L}_{pathology} \quad \xrightarrow{T_2} \quad \mathcal{L}_{organ}$$

$T_1$ being the voxelization of the organs surface, $T_2$ a voxel to surface conversion algorithm, e.g. Marching Cubes [12]. In the ideal case $T_2 = T_1^{-1}$, so that parts not involved in the tumor gestation process are not altered. As $T_2 \approx T_1^{-1}$, it is better to select the region of growth in $\mathcal{L}_{organ}$ and only transform this portion of the surface. $T_2$ will then produce a surface fragment that has to be merged with the remaining organ's surface. Possible collisions have to be handled appropriately. The improved procedure can be written as

$$M'_{organ} \quad \subset \quad M_{organ} \tag{1}$$

$$\mathcal{L}_{organ} \quad \xrightarrow{T_1} \quad \mathcal{L}_{pathology} \quad \xrightarrow{T_2} \quad \mathcal{L}_{organ} \tag{2}$$

$$M_{scene} \quad = \quad f_{collision}(M_{organ} \cup M_{pathology}) \tag{3}$$

where $\subset$ defines the selection of a region of interest, $\cup$ the surface merging operation, and $f_{collision}$ the handling of any collisions. This procedure explains, why the cellular automaton is not suited for the generation of polyps. A cellular automaton cannot handle collisions, since two adjacent cells of the same tissue have no information whether they belong to the same or different surface fragments. To handle collisions, equations 1, 2 and 3 would have to be applied on every growth iteration. The repeated change of representation would lead to an unacceptable accumulation of errors.

For the skeleton approach, the combination is simplified by the fact that the model already entails a surface representation. The only transformation required is

$$\mathcal{L}_{pathology} \quad \xrightarrow{T} \quad \mathcal{L}_{organ} \tag{4}$$

where $T$ represents a simple rotation and translation of the model $M_S$ to position the local coordinate system in the selected point $p$ of origin of the pathology in the organ. Equation 3 also holds for the transformed model $M_S$ to obtain a coherent surgical scene.

Merging $M_S$ and $M_{organ}$ in $\mathcal{L}_{organ}$ is more involved than in the case of the cellular automaton and will be described in more details. For simplicity of the description, equation 4 is inverted. Thus, merging is accomplished in $\mathcal{L}_{pathology}$. The final result needs to be transformed with $T$ to obtain a scene in the correct coordinate system.

The triangulation surrounding the point $p \in M_{organ}$ is refined to roughly match the resolution of the pathology's rim $\mathcal{R}_{pathology}$. The points closer to the point $p$ than the pathology's radius are removed, thereby creating a hole in $M_{organ}$ of approximately the size of the pathology's base. The resulting rim in $M_{organ}$ is denoted $\mathcal{R}_{organ}$. Image a) in Figure 2 shows an exemplary case.

The points of $\mathcal{R}_{pathology}$ and $\mathcal{R}_{organ}$ have to be connected, so that the surface triangulation is closed and no two points of the same rim are connected. That is, $m$ points of $\mathcal{R}_{organ}$ and $n$ points of $\mathcal{R}_{pathology}$ have to be mapped with the additional constraints of no overlapping connections and smallest possible distances between the connected points. The later restriction is required during the relaxation process of the springs derived from the newly created connections.

First the points on $\mathcal{R}_{organ}$ are projected on the plane $\Sigma$ by rotating them around the closest tangential segment of $\mathcal{R}_{pathology}$, so that they lie outside of the ellipse described by $\mathcal{R}_{pathology}$. The points $p_i \in \mathcal{R}_{organ}$ and $q_j \in \mathcal{R}_{pathology}$ next to each other are selected as starting points $p_0$ and $q_0$. The remaining points of each rim are sorted along the rim with the same orientation around the origin. A matrix of all possible angles between the normals $\boldsymbol{n}_j$ of the points $q_j$ and the vectors $\boldsymbol{m}_{ij} = \overrightarrow{q_j p_i}$ is constructed

$$A_{ij} = \sphericalangle(\boldsymbol{n}_j, \boldsymbol{m}_{ij}) \qquad A \in \Re^{m \times n}$$

A triangle between the two rims is now represented by two adjacent values in $A$. The global optimal triangulation in the sense stated above corresponds to the cheapest path from $A_{00}$ to $A_{mn}$. This path can be found by building a new matrix $B$ that accumulates the values in $A$ starting from $A_{00}$

$$B_{ij} = \min(A_{i,j} + B_{i-1,j}, A_{i,j} + B_{i,j-1}) \qquad B \in \Re^{m \times n}$$

and building the triangles by starting at $B_{00}$ and always selecting the lower of the adjacent values. Finally the points $q_j$ are projected back to their original positions.

The new connections are represented by springs with equilibrium length zero. These springs and the pathology's springs are relaxed to attract the pathology's surface $\Omega$ to the uterine cavity. Image b) in Figure 2 illustrates all springs connected to $\mathcal{R}_{organ}$ and $\mathcal{R}_{pathology}$ before relaxation. Image c) in Figure 2 is the result after relaxation of the springs. The boundary between the pathology's rim and the uterine cavity is no longer $\mathcal{C}^1$-continuous, as was the case with the

original virtual plane $\Sigma$. Nevertheless, as can be seen in image c) in Figure 2, this inconsistency is barely visible on the scale of interest.

The inserted pathology will very likely overlap at some places with the uterine cavity. Depending on the type of pathology, this collisions have to be dealt with differently. As argued in Section 2, myomas have a very strong tendency to keep a spherical shape. The edges of the triangles building the surface of the organ are equally modeled by springs. A collision of a myoma and the cavity will be handled by correcting the cavity's surface while fixing any point of the pathology.

In contrast to the myoma the polyp is a very soft tissue mass, which will be deformed according to the uterine cavity's shape. Only springs belonging to the pathology, both peduncle and polyp, are relaxed during collision handling. The final results of the skeleton-based approach are compared to a real polyp in Figure 3.

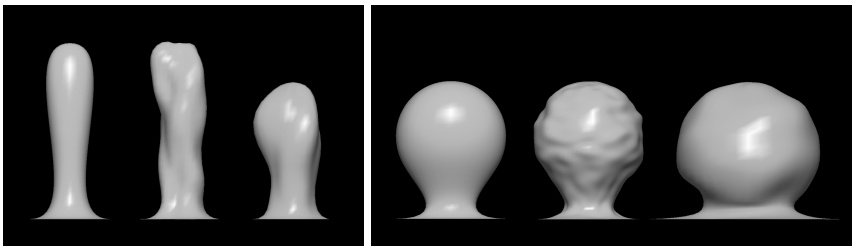

**Fig. 1.** The first image exhibits an undistorted and its corresponding distorted polyp profile, as well as a variation of the shape. The second image illustrates the corresponding profiles for myomas.

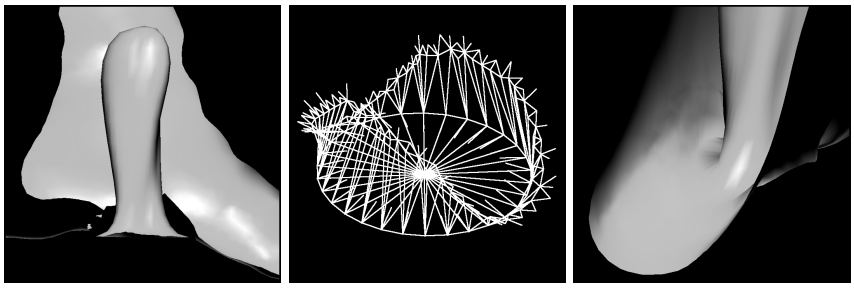

**Fig. 2.** Image a) is an example of a polyp inserted in the organ before merging. Image b) shows the resulting connections and image c) the result after relaxation of the springs.

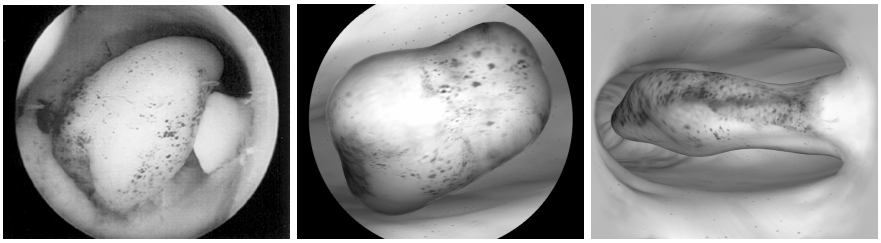

**Fig. 3.** Real polyp (left) and two different views of an artificial polyp in the uterine cavity. The cavity has been inflated to allow for a better view, as is done during surgery. The last image is an unusual perspective during actual surgery but gives an excellent overview of the scene.

## 5 Conclusion and Future Research

The presented approaches have all been discussed with a experienced gynecologists, who attested them a high resemblance with real cases. As we are aware that such validation will never overcome the limitations of subjective judgment, we are looking for long term validation strategies. This will entail the comparison of different modeling approaches as they emerge and the comparison of the resulting models during actual training with real cases, giving not only the visual, but also the haptic feedback. Future research will concentrate on the two pathologies presented.

The described approach of designing a pathology for surgical training simulators has both advantages and disadvantages over the cellular automaton. The main advantages are, that both polyps and myomas can be generated and that no growing time is required, making the generation of a pathology model possible in the order of one second. While completely autonomous generation was one of the requirements stated for the generation of pathologies for surgical training simulators, a physician might want to modify the resulting pathologies to more specifically match his expectations. The presented model is well suited for this task, as mass-spring models of this size can be modified at interactive rates.

However, some features might be missing. As an example the inner core of the myomas cannot be discerned from the surface. Therefore the generated myomas might not supply sufficient information for an accurate vascularization model.

Polyps are also a common finding in other organs, e.g. the colon (colon-rectal polyps). The described approach is completely independent of the organ chosen, allowing a direct application to any other surface-based organ model.

### Acknowledgments

This work has been performed within the frame of the Swiss National Center of Competence in Research on Computer Aided and Image Guided Medical Interventions (NCCR CO-ME) supported by the Swiss National Science Foundation.

## References


1. M. Bajka. *Empfehlungen zur Gynäkologischen Sonographie.* Schweizerische Gesellschaft für Ultraschall in der Medizin, 2001.
2. H. Blum. A transformation for extracting new descriptors of shape. *Models for the Perception of Speech and Visual Form. MIT Press*, pages 362–380, 1967.
3. Cootes et al. Active Shape Models - Their Training and Application. *Computer Vision and Image Understanding*, 61(1):38–59, 1995.
4. D'Arcy W. Thompson. *On Growth and Form, Volume I,II.* Cambridge University Press, 1952.
5. G.Farin. *Curves and Surfaces for CAGD. A practical guide.* Academic Press, San Diego, USA, fourth edition, 1997.
6. G.Székely et al. Virtual Reality-Based Simulation of Endoscopic Surgery. *Presence*, 9(3):310–333, 2000.
7. Kelemen et al. Elastic Model-Based Segmentation of 3-D Neororadiological Data Sets. *IEEE Transactions on Medical Imaging*, 18(10):828–839, 1999.
8. K.Montgomery et al. Surgical Simulator for Hysteroscopy: A Case Study of Visualization in Surgical Training. *IEEE Visualization 2001*, 2001.
9. C. Kuhn. *Modellbildung und Echtzeitsimulation deformierbarer Objekte zur Entwicklung einer interaktiven Trainingsumgebung für Minimal-Invasive Chirurgie.* Forschungszentrum Karlsruhe GmbH, Karlsruhe, 1997.
10. R. Kurman and M. Mazur. *Blaustein's Pathology of the Female Genital Tract.* Springer, Berlin, New York, fourth edition, 1990.
11. S. Kyriacou et al. Nonlinear Elastic Registration of Brain Images with Tumor Pathology Using a Biomechanical Model. *IEEE Transactions on Medical Imaging*, 18(7):580–592, 1999.
12. W. Lorensen and H. Cline. Marching Cubes: A High Resolution 3D Surface Construction Algorithm. *Computer Graphics*, 21(4):163–170, 7.1987.
13. S. Pizer et al. Multiscale Medial Loci and Their Properties. *Int. J. Comp. Vision*, accepted 2002.
14. Pschyrembel, Strauss, and Petri. *Praktische Gynäkologie für Studium, Klinik und Praxis.* de Gruyter, Berlin, New York, fifth edition, 1990.
15. R.Sierra, G.Székely, and M.Bajka. Generation of Pathologies for Surgical Training Simulators. *MICCAI*, Proceedings, Part II:202–210, 2002.
16. *Journal of Obstetrics and Gynecology of India.* http://www.journal-obgyn-india.com/issue_march_april2001/g_papers_115.htm, 2002.